

広島大学学術情報リポジトリ

Hiroshima University Institutional Repository

Title	Layered Double Hydroxide Nanocluster: Aqueous, Concentrated, Stable, and Catalytically-Active Colloids towards Green Chemistry
Author(s)	Tokudome, Yasuaki; Morimoto, Tsuyoshi; Tarutani, Naoki; Vaz, Pedro D.; Nunes, Carla D.; Prevot, Vanessa; Stenning, Gavin; Takahashi, Masahide
Citation	ACS Nano , 10 (5) : 5550 - 5559
Issue Date	2016-04-28
DOI	10.1021/acsnano.6b02110
Self DOI	
URL	https://ir.lib.hiroshima-u.ac.jp/00053540
Right	© 2016 American Chemical Society This document is the Accepted Manuscript version of a Published Work that appeared in final form in ACS Nano, copyright © American Chemical Society after peer review and technical editing by the publisher. To access the final edited and published work see https://doi.org/10.1021/acsnano.6b02110
Relation	This is not the published version. Please cite only the published version. この論文は出版社版ではありません。引用の際には出版社版をご確認、ご利用ください。

Layered Double Hydroxide Nanocluster: Aqueous, Concentrated, Stable, and Catalytically-Active Colloids towards Green Chemistry

*Yasuaki Tokudome^{*a} Tsuyoshi Morimoto,^a Naoki Tarutani,^a Pedro D. Vaz,^{b,c} Carla D. Nunes,^b*

Vanessa Prevot,^{d,e} Gavin Stenning,^c and Masahide Takahashi^a

^aDepartment of Materials Science, Graduate School of Engineering, Osaka Prefecture University, Sakai, Osaka, 599-8531, Japan. ^bCentro de Química e Bioquímica, Departamento de Química e Bioquímica, Faculdade de Ciências da Universidade de Lisboa, Campo Grande, Ed. C8,1749-016 Lisboa, Portugal. ^cISIS Facility, Rutherford Appleton Laboratory, Chilton, Didcot, Oxfordshire OX11 0QX, United Kingdom. ^dUniversité Clermont Auvergne Université Blaise Pascal, Institut de Chimie de Clermont-Ferrand, BP 10448, F-63000 Clermont-Ferrand, France. ^eCNRS, UMR 6296, ICCF, F-63171 Aubiere, France.

ABSTRACT

Increasing attention has been dedicated to the development of nanomaterials rendering green and sustainable processes, which avail in benign aqueous reaction media. Herein, we demonstrate the synthesis of a novel family of green nanomaterials, layered double hydroxide (LDH) nanoclusters, which are concentrated (98.7 g/L in aqueous solvent), stably-dispersed (transparent sol for >2 weeks), and catalytically-active colloids of nano LDHs (isotropic shape with the size of 7.8 nm by SAXS). Proof-of-concept applications revealed that the LDH nanocluster works as a solid basic catalyst and allows easy-separation from solvents of catalytic reactions, confirming the nature of nanocatalysts. The

present work closely investigates the unique physical/chemical features of this colloid, the formation mechanism, and the capability as basic nanocatalysts in benign aqueous reaction systems.

INTRODUCTION

Nanocatalysts exhibit a significant contact with reactants and allow easy-separation from products, simultaneously achieving the advantages of heterogeneous and homogeneous catalysts. Increasing attention has been dedicated to the development of nanomaterials rendering green and sustainable processes which avail in benign aqueous reaction media.¹ Layered double hydroxide (LDH), which is a family of lamellar metal hydroxides accommodating anions in their interlayers, is a promising candidate as a green catalyst. LDHs take various combinations of ubiquitous metals and anionic species; the general formula of LDHs is $[M^{2+}_{1-x}M^{3+}_x(OH)_2][A_{x/n}^{n-} \cdot mH_2O]$, where M^{2+} and M^{3+} are di and tri valent cations, and A^{n-} is anion. The tunable and distinctive properties of LDHs are surface basicity, adsorptive nature, anion exchangeability, and bio- and environmental compatibilities.^{2,3} Recent reports have demonstrated that LDH crystals with micron-scale dimensions catalyze chemical reactions in aqueous media, such as Knoevenagel condensation⁴ and CO₂ reduction.⁵ Nanocrystallization of LDH is highly demanded for more advanced and efficient processing.

In spite of the tremendous promise as nanocatalysts, aqueous synthesis of “nano-LDH” is a considerable challenge because of their rapid crystallization kinetics. In principal, nanocrystallization favorably occurs at higher supersaturation (*i.e.*, LDH synthesis at higher M^{2+} , M^{3+} , and/or OH^- concentrations),⁶ however it is inevitably accompanied by the rapid aggregation of embryonic crystals to form an inhomogeneous gel-like state. The synthesis of nano-LDH suspension in an aqueous solvent is exceptionally allowed by using micelles as a nano reaction-pool.⁷ Even in the case, the particle diameter is in tens nm and the LDH-polymer composites are obtained as a diluted suspension.

Overcoming the trade-off of the crystallization principle between synthesis and stabilization of nanocrystals is a key issue that merit important consideration to achieve LDH nanomaterials that avail in green processes. Tuning the nanomorphology will determine catalytic activity/selectivity and adsorption properties, given the fact that tailored chemical/physical properties of size, shape, and composition dictate activity and selectivity in current nanocatalysts of oxides,⁸ metals and alloys (bimetallic compounds),⁹ organic complexes, and their composites.¹⁰

The preparation of LDH nanomaterials is generally bypassed by delamination of bulky LDH crystals, instead of involving the direct synthesis at higher supersaturation.^{11,12} Bulky crystals grown at lower supersaturation are delaminated to yield two dimensional (2D) nanosheets with a thickness around one nm and a lateral dimension from submicron to tens micron.¹³ It was recently demonstrated that Aqueous Miscible Organic Solvent Treatment (AMOST) yields delaminated LDH powders maintaining their delaminated state with extremely high specific areas of 260-460 m²/g⁻¹.^{14,15} On the other hand, isolating delaminated LDH nanosheets in polar solvents is still a considerable challenge due to aggregation and restacking, imposing a need to be highly-diluted in a liquid media.^{11,16} The stability of delaminated LDH suspensions are reportedly lost in several days at a concentration as low as 10 gL⁻¹,^{17,18} and a high ionic strength and/or poor solvents involved in the real applications further decrease the stability of these colloids. To achieve stable and concentrated aqueous suspension will give benefits for the development of LDH nanocatalysts in the next generation.

Herein, we for the first time demonstrate the “direct” synthesis of nano LDH aqueous suspension, which is hereafter called as LDH nanocluster (LDH NC), by overcoming the trade-off of the crystallization principle between synthesis and stabilization at higher supersaturation. The synthesis of nano LDH was attempted at a considerably high supersaturation. Nevertheless, stable suspension without aggregation was successfully achieve by taking advantage of the spontaneous gelation-deflocculation transition of nanocrystalline LDH gels. The synthesis was performed via one pot process

from commonly available chemicals (metal chlorides, propylene oxide (PO) and, acetylacetonate (acac)) in an aqueous solvent at a room temperature. LDH NCs give extremely high solid surface area in aqueous media and the available solid surface in water exceeds those of delaminated LDHs. Simultaneously, the high stability of the LDH NC allows easy separation from the products after the catalytic reactions. The unique physical/chemical features of this colloid, the formation mechanism, and the capability as basic nanocatalysts in benign aqueous reaction systems will be closely discussed.

EXPERIMENTAL SECTION

Chemicals. Nickel (II) chloride hexahydrate ($\text{NiCl}_2 \cdot 6\text{H}_2\text{O}$: 98%), aluminum chloride hexahydrate ($\text{AlCl}_3 \cdot 6\text{H}_2\text{O}$: 98%), iron (III) chloride hexahydrate ($\text{FeCl}_3 \cdot 6\text{H}_2\text{O}$: 99%), iron (II) chloride tetrahydrate ($\text{FeCl}_2 \cdot 4\text{H}_2\text{O}$: 99%), hydrochloric acid (HCl: 35-37%), sodium hydroxide (NaOH: 97%), citric acid (H_3Cit : 98%), ethanol (EtOH: 99.5%), toluene (99%), and acetylacetonate (acac: >99%) were purchased from Wako Pure Chemicals Industries. Propylene oxide (PO: $\geq 99\%$), pluronic F127, benzaldehyde (> 99%), *Cis*-cyclooctene (95%), styrene ($\geq 99.5\%$), *R*-(+)-limonene (97%), *trans*-hex-2-en-1-ol ($\geq 95\%$), *tert*-butylhydroperoxide (TBHP: 5.5 M in decane), cumene hydroperoxide (CHP: 80%), dibutyl ether (99.3%), and decane ($\geq 99\%$) were purchased from Sigma-Aldrich Co. Malononitrile (> 98%) and ethyl cyanoacetate (> 99%) were purchased from Tokyo Chemical Industry Co. LTD. All the chemicals were used as received.

Synthesis of LDH NC. The typical synthesis of LDH NC is as follows. $\text{NiCl}_2 \cdot 6\text{H}_2\text{O}$ (0.594 g; 2.50 mmol) and $\text{AlCl}_3 \cdot 6\text{H}_2\text{O}$ (0.302 g; 1.25 mmol) were dissolved in a mixture of EtOH (1.50 mL; 25.7 mmol) and ultra pure water (1.00 mL; 55.6 mmol), followed by acac addition (130 μL ; 1.25 mmol). After stirring for >30 min in a glass closed container at a room temperature ($\sim 20^\circ\text{C}$), PO (1.31 mL; 18.7 mmol) was added to the mixture and further stirred for 1 min to yield a homogeneous solution. Then, stirring was stopped, and the container was sealed and kept at a room temperature ($\sim 20^\circ\text{C}$). The

mixture changed into a gel in ~2 h and deflocculated in ~7 h. The molar ratio in the reaction solution was Ni^{2+} : Al^{3+} : acac: H_2O : EtOH: PO = 2: 1: 1: 44.5: 20.6: 15.0.

Fabrication of LDH Films and Powders. *LDH Films:* LDH NC was spin-coated on precleaned Si and silica substrates at 2000 rpm and dried at 60 °C. *Mesoporous LDH Powders:* LDH NC mixed with Pluronic F127 was casted on a petri dish, dried at 100 °C under a reduced pressure, and heated at 250 °C to remove F127. *Macroporous LDH films:* 0.005 wt% of aqueous polystyrene (PS) suspension ($D = 0.10 \mu\text{m}$, 5010A, Latex Microsphere Suspensions 10 wt%, Thermo Scientific) was drop-casted on a Si substrate and allowed to self-assemble into an opal film through the coffee stain effect¹⁹ at 20 °C and 50%RH. LDH NC was 10-fold diluted with EtOH and spin-coated on the PS opal film at 8000 rpm for 60 s. The film was heat treated at 150 °C for 24 h. PS was chemically etched by chloroform (>99%, Wako Pure Chemicals Industries) to yield an inverse opal LDH film. *Magnetic LDH particles:* Magnetic particles were prepared according to a previous report.²⁰ $\text{FeCl}_3 \cdot 6\text{H}_2\text{O}$ (5.44 g) and $\text{FeCl}_2 \cdot 4\text{H}_2\text{O}$ (2.00 g) were dissolved in a mixture of ultrapure water (50 mL) and 1 M HCl aq. (10 mL). This solution was added drop by drop to 100 mL of 1 M NaOH aq. under stirring at room temperature in a N_2 atmosphere, which changed the color of solution from yellow to black. The solution was further stirred for 30 min to yield magnetic maghemite ($\gamma\text{-Fe}_2\text{O}_3$) nanoparticles. $\gamma\text{-Fe}_2\text{O}_3$ nanoparticles were centrifuged and washed 5 times with ultrapure water. Thus obtained $\gamma\text{-Fe}_2\text{O}_3$ nanoparticles were dispersed in 500 mL of ultrapure water (1.42 mg/mL). 0.1 g of H_3Cit was added to 10 mL of the $\gamma\text{-Fe}_2\text{O}_3$ suspension, stirred for 1 min. 1.875 mL of suspension of H_3Cit -modified $\gamma\text{-Fe}_2\text{O}_3$ nanoparticles (H_3Cit -magNP) was mixed with 30 mL of LDH NC (3 mg/mL, purified by dialysis in ion exchanged water) to yield magnetic LDH NC.

Characterization. A field emission scanning electron microscope (FE-SEM; S-4800, Hitachi, with a thin Pt/Pd coating) and transmission electron microscopes (TEM; JEM-2000FX, JEOL, Japan and Hitachi 7650, Hitachi, Japan) were employed to observe fine structures. Crystalline nature of the film was identified by X-ray diffraction (XRD; SmartLab and Maltiflex, Rigaku) using $\text{CuK}\alpha$ radiation ($\lambda =$

0.154 nm). The micro/mesopore characteristics of the samples were analyzed by N₂ sorption measurements (Belsorp-mini II, Bel Japan Inc., Japan). Prior to N₂ sorption measurements, samples were outgassed under vacuum at 200 °C. Thermogravimetric-differential thermal analysis (TG-DTA; Thermo Plus Evo, Rigaku, Japan) was carried out at a ramp rate of 10 °C min⁻¹ while continuously supplying air at a rate of 300 mL min⁻¹. Liquid state ¹H NMR measurement was performed with JEOL JNM-ECS400 spectrometer to assess the progress of Knoevenagel condensation. Ultraviolet-visible (UV-Vis: V-670 spectrophotometer, JASCO Corp.) was used to assess the chelation of acac molecules. Inductively coupled plasma (ICP: ICPS-8000, Shimadzu Corp.) emission spectroscopy was employed to analyze the chemical composition of the colloidal solution. The LDH NC was centrifuged at 450,000 rpm for 210 min, and a supernatant and a precipitate were dissolved by HCl and analyzed, respectively. Zeta-potential and size distribution of LDH NC (based on dynamic light scattering) were measured with a nano Zeta-sizer (Malvern instruments, LTd, UK) apparatus, using a laser Doppler electrophoresis (LDE). The magnetic property of the particles was assessed with a SQUID (MPMS XL-7, Quantum Design, Inc, USA) by measuring a hysteresis loop with applied fields +/- 7 T at 300 K. Small-angle X-ray scattering (SAXS) (SmartLab, Rigaku, λ = 0.154 nm) was performed on LDH NC to investigate the morphology and agglomeration state of the LDH nanocrystals. The scattering profiles were plotted against the scattering vector, *q*, where *q* is related to the scattering angle, 2θ, and the wavelength of X-ray irradiation, λ, through

$$q = (4\pi/\lambda) \sin\theta \quad (1)$$

SAXS curves were fitted with Irena package²¹ by the unified equation proposed by Beaucage and Schaefer,^{22,23} which was developed to describe scattering from objects with a hierarchical structure, *i.e.*, primary particles and their aggregates in the present case.

$$I(q) \approx \sum_{i=1}^n \left(\frac{G_i \exp(-q^2 R_{gi}^2)}{3} + \frac{B_i \exp(-q^2 R_{g(i+1)}^2)}{3} \left\{ \frac{[\text{erf}(q R_{gi}/\sqrt{6})]^3}{q} \right\}^{P_i} \right) \quad (2)$$

where n is the number of structure levels, R_{gi} is the radius of gyration of the i th level, P_i is the power-law exponent, G_i is the Guinier prefactor, and B_i is the prefactor specific to the type of power-law scattering falls. In the present study, n was set at 1 or 2, corresponding the structural models of primary particles without and with aggregation, respectively. The reaction solution was well-fitted with $n = 1$ at $t < 2$ and $7 \text{ h} \leq t$ since PO addition, whereas $n = 2$ (or $n > 2$) gave better fitting during the temporal gelation and deflocculation, $2 \text{ h} \leq t < 7 \text{ h}$. In-situ XRD and SAXS was performed a sample encapsulated in a rotating capillary.

Catalytic studies. *olefin epoxidation:* 7.3 mmol of each substrate (*Cis*-cyclooctene, styrene, *R*-(+)-limonene, *trans*-hex-2-en-1-ol), 2.650 mL of *t*-BuOOH (TBHP: 5.5 M solution in decane, 14.6 mmol), and 0.127 mL of LDH NC (0.073 mmol of Ni), were reacted without solvent or adding 2 mL of decane. Dibutyl ether (equivalent gram with the substrate) was added as an internal standard. The mixture was reacted at 120 °C in a closed vessel under stirring at 500 rpm. Conversion and product yield were monitored by sampling periodically at 10, 30 min, and 1, 1.5, 2, 4, 6, 8 and 24 h. These samples were treated as described previously prior to injection in the GC column.²⁴ The course of the reactions was monitored by quantitative GC analysis performed using a Shimadzu QP2010-Plus GC/MS system and a capillary column (Teknokroma TRB-5MS or TRB-1MS) operating in the linear velocity mode. *Knoevenagel reaction:* LDH NC was purified via dialysis against ion exchanged water (2 L) with a dialysis tube (MWCO = 15kD (#132562), Spectrum Laboratories, INC). Ion exchanged water was replaced with fresh water in 8 h, and then replaced another 3 times every 24 h. A mixture of LDH NC (25 mg), benzaldehyde (0.5 mmol), ethylcyanoacetate (0.5 mmol), and water (50 mL) was stirred at a room temperature in a closed container. The kinetic plot was obtained by measuring time-dependence of an absorption peak of benzaldehyde. 0.2 mL of reaction solution was collected through a filter ($\phi = 0.45 \mu\text{m}$), 10-fold diluted with EtOH, and the decrease of adsorption band at $\lambda = 245 \text{ nm}$ was analyzed by UV-Vis spectroscopy. The conversion was estimated by liquid state ^1H NMR. Assignments of ^1H NMR spectra: benzaldehyde: δ 10.03 (s, 1H), 7.90 – 7.87 (m, 2H), 7.66 – 7.52 (m, 3H); ethy

cyanoacetate: δ 4.30 – 4.25 (q, 2H), 3.45 (s, 2H), 1.35 – 1.31 (t, 3H); benzalmalononitrile: δ 7.92 – 7.90 (m, 2H), 7.78 (s, 1H), 7.66– 7.53 (m, 3H); Malononitrile: δ 3.59 (s, 2H).

RESULTS AND DISCUSSION

The synthesis and characterization of LDH nanocluster

LDH nanocluster (LDH NC) was synthesized via a facile one-pot route at a room temperature in air atmosphere from commonly available chemicals. Briefly, $\text{NiCl}_2 \cdot 6\text{H}_2\text{O}$ (0.594 g; 2.50 mmol), $\text{AlCl}_3 \cdot 6\text{H}_2\text{O}$ (0.302 g; 1.25 mmol), acetylacetone (acac) (130 μL ; 1.25 mmol) were dissolved in a mixture of EtOH (1.50 mL; 25.7 mmol) and ultra pure water (1.00 mL; 55.6 mmol). Then, propylene oxide (PO) (1.31 mL; 18.7 mmol) was added and left at a room temperature for 24 h. Without any additional processes, green-colored colloidal suspension which exhibits the Tyndall effect was spontaneously formed (**Figure 1a**). **Figure 1b** shows XRD pattern of powders collected from the suspension. The diffraction pattern is ascribed to hydrotalcite-type LDH with rhombohedral (R3m) symmetry. d_{003} is calculated as 7.76 Å ($2\theta = 11.4^\circ$) and (003) crystallite size is estimated as 5.4 nm by the Scherrer's equation. The crystals possess an isotropic shape with a diameter of ~ 5 nm as observed in FE-SEM and TEM images (**Figures 1c and S1**). The size distribution of LDH LC is small without abnormally-grown crystallites. The synthesis condition of LDH NC exhibits a significant contrast with those of standard micron-sized LDHs. The synthesis of micron-sized LDHs is reportedly performed at a low supersaturation (at a low metal concentration) of 10 mM to grow crystals without aggregation.²⁵ In contrast, LDH in the present case was synthesized at a highly concentrated starting solution of 826 mM to achieve a high supersaturation, allowing to induce the nanocrystallization. Nevertheless, SAXS analysis coupled with theoretical fitting based on the unified equation²² demonstrated that individual

crystal with a diameter of 7.8 nm was isolated in the suspension without aggregation (**Figure 1d**) (the reaction mechanism is discussed in the next section). The narrow particle size distribution is also supported by dynamic light scattering measurements (**Figure S2**). The distribution curves which are centered at ~8 nm also confirms the formation of monodispersed particles without aggregation. Inductively coupled plasma (ICP) emission spectroscopy and TG-DTA analysis revealed that LDH NC, with a chemical composition of $\text{Ni}_2\text{Al}(\text{OH})_6 \cdot 1.5\text{H}_2\text{O} \cdot \text{acac}$, was obtained at a yield of >93%. To the best of our knowledge, the present LDH NC is the smallest LDH obtained as an aqueous colloid without aggregation. A previous report demonstrated the preparation of LDH particles with the dimension of 10 nm under a nonhydrous condition using tris(hydroxymethyl)aminomethane (THAM) as a ligand.²⁶ On the other hand, aqueous reactions have not achieved LDHs with a lateral dimensions below 50~60 nm.^{7,27,28} We can conclude that the present method successfully overcomes the trade-off between the synthesis and the stabilization of nanocrystals in water, and thereby LDH nanocrystals with 7.8 nm and a high stability (> 2 weeks) is obtained at a high yield (93 %).

The concentration of LDH NC is 98.7 g/L, 10-100 times higher compared to suspensions of exfoliated LDH nanosheets. At 100 gL^{-1} , exfoliated LDHs reportedly form turbid inhomogeneous gels upon mixing with a liquid.¹⁸ An accessible solid surface area of exfoliated LDH nanosheets suspended at 5 g/L in an aqueous solvent is estimated as $2.3 \text{ m}^2/\text{mL}$,²⁹ whereas that of LDH NC with a high concentration of 98.7 g/L is estimated as $32 \text{ m}^2/\text{mL}$.³⁰ The comparison as a suspended form demonstrates that the present LDH NC offers 14 times larger surface area than exfoliated LDH nanosheets. The crystallization of massive LDH NC is a significant advantage over LDHs obtained by electrochemical deposition (ED). ED is alternative way to yield nanocrystalline LDH, however the occurrence of nucleation and growth is limited on a surface of electrodes, limiting in the synthesis of LDH thin films with a small sample mass.³¹ The extremely high concentration as well as the

nanocrystallinity of LDH NC is a critical advantage for practical applications, including adsorption and catalytic applications as demonstrated later.

LDH NC formed a homogeneous gel simply by drying at a room temperature or heating at 100 °C, without inhomogeneous precipitation and aggregation. **Figure S3** shows a homogenous gel obtained by heating at 100 °C in a closed vessel. The capability of gelation allows further processing starting from LDH NC. Smooth films with a thickness between 20 nm to 400 nm could be obtained by a single coating (**Figure S4**). The transparent LDH thin films are desirable for fundamental researches as well as advanced applications in photochemical and electrochemical fields.^{32,33} Moreover, coupled with templating methods widely used in sol-gel chemistry, meso and macroporous pure LDHs materials, which are so far difficult to achieve, could be fabricated from LDH NC. Well defined macroporous structure with a pore diameter of 80 nm was obtained via hard templating with PS spheres (**Figure 1e**). The templated macropores are far smaller than previous hard-templated LDHs (>420 nm).³⁴ Pluronic F127, block copolymer, was also available as a porogen to increase a specific surface area. The IV type isotherm with a hysteresis in the case of F127 incorporated clearly demonstrate mesoporosity (**Figure S5**). BET surface area is as high as 322 m²g⁻¹, which is comparable to delaminated powdery LDHs prepared by AMOST. Assuming the particle is spherical with a density of Ni(OH)₂, 4.1 g/cm³, the BET surface area of 322 m²g⁻¹ gives an average crystal diameter of 4.5 nm which is in good agreement with the values from other analyses including SAXS and TEM.

In summary, the preparation of LDH NC is successfully achieved by overcoming the trade-off between the synthesis and the stabilization of nanocrystals in water. LDH NC was used as nanobuilding blocks towards meso and macroporous structured LDHs as well as smooth LDH films. These tunable structured LDHs are desirable for the applications in biochemistry, storage, catalysis, and energy conversion.

The formation mechanism of LDH nanocluster

LDH NC formed through a spontaneous gelation-deflocculation process. **Figure 2a** shows the time evolution of the reaction mixture at 1, 4, and 24 h since PO addition ($t = 0$). The reaction sol became an opaque gel at $t = 2$ h and deflocculated at $t = 7$ h, which is induced by a successive increase of pH of the reaction mixture. PO works as a proton scavenger through the protonation of the epoxide oxygen and the subsequent ring opening reaction by the nucleophilic attack of conjugate bases, such as H_2O or Cl^- .³⁵ The protonation and ring opening reactions leads to the increase of solution pH (**Figure 2b**). The value of pH increased rapidly from 0.4 (at $t = 0$ min) to 4.3 at $t = 5$ min, then gradually increased to 8.9 at $t = 12$ h, and reached to 9.6 at $t = 24$ h. The rapid increase of pH in the initial stage forms massive $\text{Al}(\text{OH})_3$ embryos and the subsequent slower pH increase allows LDH crystallization via coprecipitation, which is supported by the corresponding XRD patterns as a function of t (**Figure 2c**). No diffraction peak is observed at $t < 2$ h, where $\text{Al}(\text{OH})_3$ amorphous nanoparticles formed (diameter = 3.3 nm by SAXS). In **Figure 2c**, (003) and (110) diffractions of hydrotalcite-type LDH were confirmed at $t = 2$ h, and (003) diffraction became prominent with the increase of t . The results demonstrate that the transient gelation shown in **Figure 2a** is accompanied with the crystallization of LDH, and the crystal growth of LDH continued until after the deflocculation.

We found that the addition of acac is the key to achieve the gelation-deflocculation transition. **Figure S6a** shows XRD patterns of the reaction mixture without incorporating acac. The crystallization of LDH was faster compared to the case with acac and almost completed at $t = 4$ h. The mixture without acac formed opaque gel at $t = 6$ min and did not deflocculate at the later stage of the reaction (**Figure S6b**). The reaction without acac is a typical gelation process taking place under at high supersaturation; $\text{Al}(\text{OH})_3$ formed a gel network on which LDH crystals coprecipitated (**Figure S6c**).^{36,37} Even when the metal concentrations were considerably decreased toward avoiding agglomeration, LDH NC did not form without acac because of aggregation or sedimentation (**Figure**

S7). These results suggests that acac plays a primal role to overcome the trade-off between the synthesis and the stabilization of nanocrystals.

The formation mechanism of LDH NC was further investigated by in-situ SAXS measurement (**Figure S8**). **Figure 3a** shows mass fractal dimension, d_f , of the primary particles estimated from Porod slope, P , at high q regime of SAXS curves, with a equation of $d_f = P$ ($0 \leq P \leq 3$). The value of d_f reflects the bonding density of the hydroxide network; higher d_f corresponds to a more densely-packed hydroxide network. acac retard the increase of d_f at the initial stage of the reaction ($t < 4$ h). At $t = 4$ h, $d_f = 1.8$ and 2.1 for the cases with and without acac, respectively. The value of d_f became saturated in ~ 9 h for the case without acac ($d_f = 2.4$ both at $t = 9$ h and $t = 168$ h), whereas it continuously increased for the case with acac ($d_f = 2.6$ at $t = 24$ h and $d_f = 2.8$ at 168 h). The time dependence of d_f suggests that the incorporation of acac form less-branched $\text{Al}(\text{OH})_3$ network at the initial stage and crystalize LDH more progressively at later stages of the reaction. Since $\text{Al}(\text{OH})_3$ is an amphoteric hydroxide, the less-branched $\text{Al}(\text{OH})_3$ is readily dissolved at a high pH at the later stage of the reaction, allowing to deflocculate and form LDH NC. Moreover, Al^{3+} supplied to the reaction mixture by the dissolution of $\text{Al}(\text{OH})_3$ was consumed to crystalize LDH. As a result, the crystallization of LDH at the later stage of the reaction occurs more progressively for the case with acac compared to without acac (**Figures 2c, S6a, and 3a**). The above discussion is also supported by time evolution of pH of reaction solutions with and without acac, as closely discussed in Supplementary Information (**Figure S9**).

UV-Vis spectroscopy was used to assess the change of acac chelation to different metal centers; π - π^* transition of a β -diketonato complex depends on its central metal.^{38,39} **Figure 3b** shows UV-Vis spectra of acac coexisting with $\text{Al}(\text{OH})_3$, $\text{Ni}(\text{OH})_2$, and LDH NC. Acac in ultra-pure water exhibited an absorption peak at 274 nm. Upon the chelation to different metal centers, the peak shifted to 283 nm for $\text{Al}(\text{OH})_3/\text{acac}$ and 297 nm for $\text{Ni}(\text{OH})_2/\text{acac}$. The reaction solution of LDH NC/acac exhibited absorption peaks at 280 nm, $t = 10$ min and at 297 nm, $t = 24$ h. These results suggest that 1) acac

coordinated to Al center in the initial stage such that the hydrolysis and condensation reactions of $\text{Al}(\text{OH})_3$ were retarded and 2) after the deflocculation, the coordination switched to Ni sites of LDH NC, giving the extremely high stability of LDH NC. It is well known that acac forms a complex more preferentially with Al^{3+} than Ni^{2+} and Al-acac complex is a major product in the acidic condition. On the other hand, Ni-acac complex is allowed to form at neutral or basic conditions.⁴⁰ The selectivity of Ni(II)-complex over Al (III)-complex increases with increasing pH.⁴¹ As a result, the coordination of acac was switched with increasing t , which is a key to the deflocculation of $\text{Al}(\text{OH})_3$ and stabilization of nano LDHs.

The formation mechanism of LDH NC is summarized in **Figure 3c**. Just after PO addition ($t < 5$ min), $\text{Al}(\text{OH})_3$ with a less-branched polymeric structure is formed with the aid of acac chelation. LDH crystalize on $\text{Al}(\text{OH})_3$ via coprecipitation in $t = \sim 2$ h, which accompanies gelation to form a $\text{Al}(\text{OH})_3$ /LDH composite gel. $\text{Al}(\text{OH})_3$ with acac is allowed to dissolve due to its amphoteric nature and less-branched polymer network, which induces deflocculation and recovers the original sol state at $t = 7$ h. The dissolved $\text{Al}(\text{OH})_3$ is consumed to crystalize LDH crystals which are then stabilized by acac adsorption on the surface of LDH crystals. As a result, the optimized reaction kinetics based on multi functionality of acac allow to yield the concentrated LDH NC with a high stability via a simple one pot process from commonly available chemical sources.

Controllable particle size and stability of LDH nanocluster

The ratio of acac to the metal sources (Ni^{2+} and Al^{3+}) is critically important for the preparation of LDH NC. **Table 1a** summarizes crystallite size, presence of impurity phases, and appearance of the mixture at $t = 24$ h as a function of acac/Al. LDH without any crystalline impurities were obtained at $\text{acac/Al} < 1.5$ and acac complexes precipitated at acac/Al ratio of ≥ 1.5 (**Figure S10**). On the other

hand, the deflocculation and the formation of LDH NC occurred at $\text{acac}/\text{Al} \geq 0.75$. Pure LDH NC was obtained in the range between $0.75 \leq \text{acac}/\text{Al} < 1.5$, where hydrolysis and condensation reactions of $\text{Al}(\text{OH})_3$ were optimized and simultaneously LDH crystallization preferably occurs rather than the competitive crystallization of metal-acac complexes. The crystallite size of LDH was tunable in single-nm scale between 3.6 and 7.1, depending on the concentration of the salutes in the starting solutions (**Table 1b**). The crystallite size decreases with decreasing supersaturation, suggesting that massive embryonic $\text{Al}(\text{OH})_3$ as a scaffold for the coprecipitation of LDHs form almost equally under these conditions, and the decrease of feeding metal sources leads to yield the smaller crystals. LDH NC is highly stable and sedimentation did not occur by applying centrifugal field of 400,000 g. The zeta potential of the LDH NC is + 31 mV, which is not so high considering the extremely high stability of LDH NC. The high stability is due to the acac modification on the LDH surface as well as the extremely small size of the particles; indeed, the dissociation of acac from the LDH NC by heating (**Figure S11**) resulted in gelation. The concentrated LDH NC can be diluted by EtOH or H_2O to increase the stability of the suspension. Four-fold dilution increases the stability at a room temperature more than 3 months (**Table 1c**). It should be emphasized that the concentration of LDH is as high as 25 mg/mL even after the four-fold dilution.

Capability of LDH NC as green nanocatalyst

Green synthesis of catalysts from ubiquitous elements/precursors has been a topic of interest in this decade.^{42,43} LDH NCs can be synthesized from a commonly available chemicals in aqueous solvents, making them promising candidates as green nanocatalysts. The basic nature of LDH NC is qualitatively assessed by the coloring of phenolphthalein (**Figure S12**). The absorbed phenolphthalein was colored on LDH NC and simultaneously confined in a dialysis tube differently from ionic or

molecular bases, confirming that the stable nanocrystals possess surface with a considerable basicity (pH for coloring is 8.3~10).

The basic nature of LDH NC was further assessed by Knoevenagel reaction. **Figure 4a** shows kinetic plots of Knoevenagel condensation in water between benzaldehyde and ethylcyanoacetate with and without Ni-Al LDH NC; for the purpose of following the time evolution, LDH NC was set at a low concentration such that the reaction occurred relatively slowly. The comparison confirms that LDH NC properly worked as basic catalysts and no induction period was observed thanks to the homogenous mixing with reactants. The conversions at 24 h were 89 % and 21 % for the cases with and without LDH NC, respectively. It should be highlighted that acac modification giving the high stability of LDH NC does not preclude the catalytic reaction. As a result, a hydrophobic sedimentation of the product was separated from the aqueous solvent containing LDH NC (**Figure 4b**). The effects of different substrates and solvents were investigated and the resultant conversions are summarized in **Table S1**. The reactions could be catalyzed in H₂O and EtOH for ethylcyanoacetate and malononitrile, whereas the activity is negligible in toluene. The catalytic activity of LDH NC is higher compared to standard Ni-Al LDHs; standard Ni-Al LDH catalyst⁴⁴ without calcination exhibited a conversion of 15% under the condition of **entry 3** of **Table S1** (**entry 3** shows a conversion of 91 %). Another study⁴⁵, which investigated a solvent-free reaction of ethylcyanoacetate with a LDH catalyst, reported a conversion of 35%, whereas the corresponding conversion in the present study is 94% (**entry 7** in of **Table S1**). Further enhancement of the catalytic activity is reportedly possible by optimizing anion species in interlayers, composition of hydroxide layers,⁴⁶ size and shape of crystals,⁴⁷ substrates,³ and heat treatment (effects of rehydration).⁴ Generally, clusters of noble metal and ligands, and enzymes have been investigated as catalysts for Knoevenagel condensation in aqueous media.⁴⁸ On the other hand, a family of LDHs is an alternative promising candidate because of the capability of using ubiquitous elements as well as their strong basic nature compared to competitive catalysts, such as X zeolites and

sepiolites.⁴⁹ The green synthesis and stabilization nanoparticles demonstrated in the present study will open up the possibility of LDH as nanocatalysts.

From another aspect, we also assessed a capability of catalytic oxidation of olefins with LDH NC. Olefin oxidation lies at the heart of the modern chemical industry and is widely used to synthesize final products, such as paints, resin, surfactants, and also intermediates in many organic reactions.^{50,51} There is a pressing need to design stable catalysts, that can selectively oxidize higher alkenes through an environmental-friendly approach.⁵² LDH is expected as a catalyst and a host for the epoxidation of renewable resources, such as vegetable oils and their fatty derivatives.^{3,53,54} **Figure 4c** summarizes the result of epoxidation of various olefins with TBHP and LDH NC as an oxidant and a catalyst, respectively. No reaction took place in the absence of catalyst, whereas LDH NC successfully catalyzed the reactions. **Figure 4c** confirms that all olefins were converted with TBHP, in the presence of LDH NC as catalyst, to their corresponding epoxides (with the exception of *trans*-hex-2-en-1-ol (**entry 4**)) with high selectivity. For *cis*-cyclooctene (**entry 1**) and *R*-(+)-limonene (**entry 3**), the catalyst converted these olefins yielding exclusively to the corresponding epoxides (100% selectivity) and 53% and 35% conversion respectively without the presence of additional solvent. The catalyst converted styrene (**entry 2**) very efficiently yielding the epoxide with 83% conversion and 69% selectivity, once again without the use of added solvent to the catalytic reaction. These achievements make it one of the best catalysts when compared with others reported in the literature; many catalysts with metal centers converted styrene with high conversion but with low selectivity towards the epoxide, yielding benzaldehyde instead.^{55,56} The epoxidation of *trans*-hex-2-en-1-ol (**entry 4**) did not yield the corresponding epoxide, however the aldehyde was formed with 100% selectivity. The high selectivity of reactions renders it further possibilities for chemical transformations using the olefin moiety (C=O). The above results were obtained without the addition of extra solvent (only decane from 5.5 M TBHP). Further addition of decane (2 mL) and thereby

decrease of the concentration of the reactants affected substrate conversion, whereas the product selectivity did not suffer any changes (**Table S2**).

The scope of the catalyst was also screened for its activity towards different oxidants. Cumene hydroperoxide (CHP) was used instead of TBHP (**Table S3**). For all substrates, the results obtained with CHP outperformed those of TBHP in what concerns substrate conversion. Overall, the product selectivity was not affected which again evidences the good performance of the catalyst. To this end, the only exception was styrene. The catalyst presented a very high conversion with CHP (97%) (**entry 2 in Table S3**), confirming that it is a very promising catalyst for styrene oxidation. Such achievements attest not only the wide scope of the catalyst, but the potential to tune chemoselectivity of the process, as well, by picking the right reaction components. Furthermore, these results pave the way for new applications of this catalyst that are currently being explored.

Finally, we demonstrate the collection and sterilization of the nanocatalyst. Magnetic LDH NC was prepared by complexing LDH with γ -Fe₂O₃ nanoparticles (magNPs).⁵⁷ γ -Fe₂O₃ modified with H₃Cit possess a highly negative charge on the surface with an isoelectric point of pH <3.⁵⁸ H₃Cit-modified magNPs readily formed a nanocomposite with LDH NC via an electrostatic interaction by simply mixing these two solutions, thanks to the inherent positive charge of LDH. The ferromagnetic property of magNPs is maintained through the process (**Figure S13**). As a result, the magnetic collection, which is one of the vital aspects in catalytic synthesis,¹ is allowed for LDH NC (**Figure 4d**). From another aspect of using LDH NC, the extremely small size of LDH NC allows sterilizing filtration which is a mandatory step for biomedical applications, such as drug-delivery and cellular uptake.⁷ **Figure S14** shows UV-vis spectra of LDH NC before and after the membrane filtration with pore diameter = 0.20 μ m. LDH NC completely pass through the membrane which blocks standard micron-sized crystals. The result demonstrated that contaminations of fungi and virus can be eliminated from LDH NC, opening up novel biomedical applications of biocompatible LDH.

CONCLUSIONS

Hydrotalcite-type LDH with an average diameter of 7.8 nm was obtained as a highly-concentrated and stable aqueous suspension (98.7 g/L). LDH NC with a controllable crystallite size between 3.6 and 7.1 nm exhibits extremely large accessible surface area in aqueous media due to its small crystallite size and high dispersivity. LDH NC can be used as nanobuilding blocks to yield mesoporous and macroporous LDHs through templating techniques, as well as transparent thin films. The reaction pathway involves the transient gelation followed by the deflocculation, which simultaneously achieve nanocrystallization and dispersion under the highly-supersaturated condition. The addition of acac and the amphoteric nature of $\text{Al}(\text{OH})_3$ play critical roles in the reaction. Optimized kinetics allowing to form pure LDH NC was achieved in the compositional range of $0.75 \leq \text{acac}/\text{Al} < 1.5$. Thus obtained LDH NC catalyze Knoevenagel condensation and olefin epoxidation. The catalytic activity is comparative or higher compared to the cases of using standard LDHs. The nanocrystals were functionalized with magnetic nanoparticles by taking advantage of inherent positive charge on the surface of LDH crystals. The magnetically modified LDH NC could be collected by a magnet, which is a vital aspect for catalytic applications. The nanocatalytic nature of LDH NC is expected to open up applications in the field of catalysis and biomedical thanks to versatilities of shape, size, and composition (intercalated anion and metal in hydroxide sheets) of LDHs. As preliminary results, we have also succeeded to obtain Co-Al and Li-Al types LDH NCs and further detailed studies on respective systems and applications of these nanocrystals are in progress.

ASSOCIATED CONTENT

Supporting Information

The Supporting Information is available free of charge on the ACS Publications website

AUTHOR INFORMATION

*tokudome@mtr.osakafu-u.ac.jp

Notes

The authors declare no competing financial interest.

ACKNOWLEDGEMENTS

The present work is partially supported by JSPS KAKENHI and JSPS-MAE SAKURA program. Y. T. appreciate financial support from the Foundation for the Promotion of Ion Engineering. CDN and PDV thank to FCT, POCI and FEDER (UID/MULTI/00612/2013) for financial support. We thank Prof. Kiyofumi Katagiri, Hiroshima University, for super-centrifuge of the colloidal suspension and Dr. Cristina I. Fernandes, Universidade de Lisboa, for the epoxidation of olefins. Special thanks go to Profs. Ogawa and Nomoto, Osaka Prefecture University, for their help for ^1H NMR measurement. Y. T. also thanks to Dr. Christine Mousty, Clermont Université, Université Blaise Pascal, for helpful discussion.

Figures

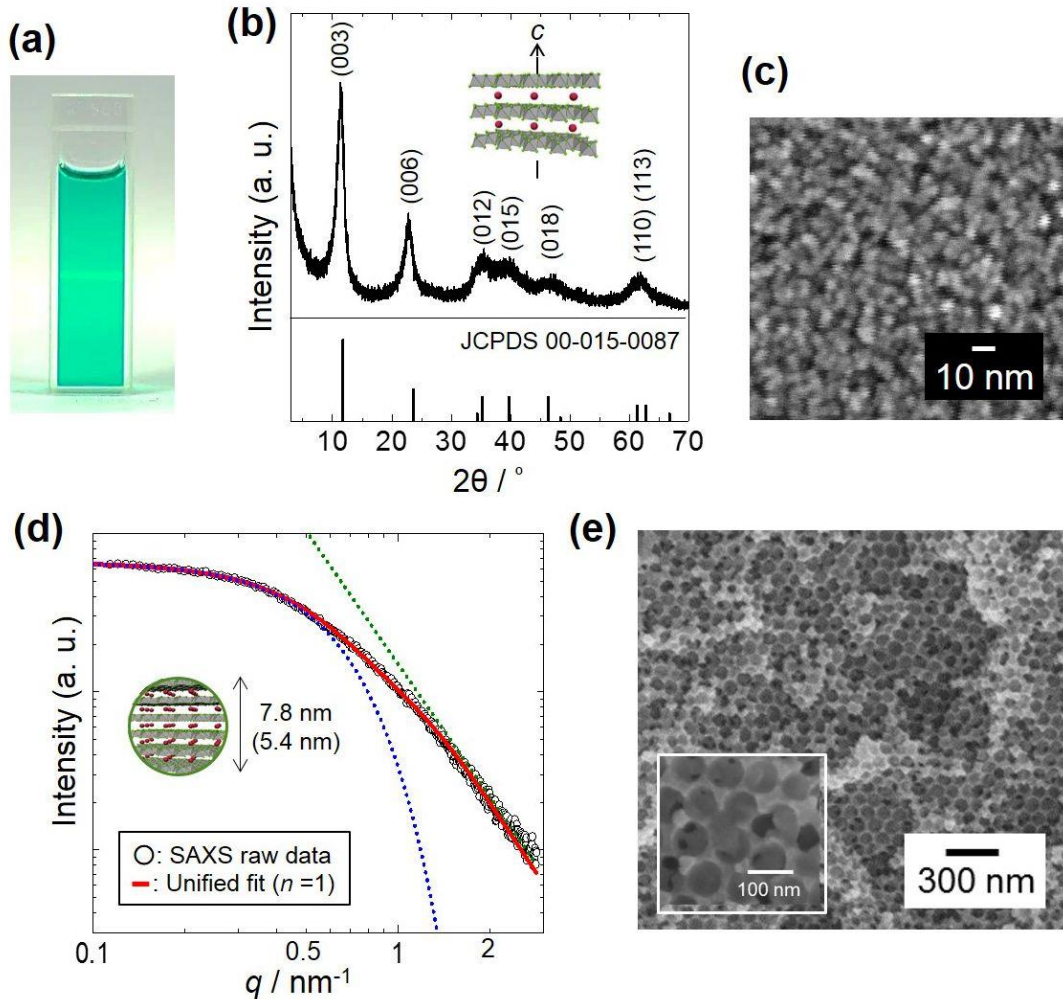


Figure 1. (a) Appearance of LDH NC. The incident light beam enters from the side of the container. (b) XRD pattern of LDH NC collected by drying. The referential data is $\text{Ni}_6\text{Al}_2(\text{OH})_{16}(\text{CO}_3, \text{OH}) \cdot 4\text{H}_2\text{O}$. (c) FE-SEM image of the LDH NC after dialysis. (d) SAXS raw data and fitting curve with the unified equation (2) at $n=1$. The blue and green dotted lines depicts 1st (Gunier) and 2nd (Porod) terms of equation (2), respectively. The inset illustration represents an envisaged LDH NC. (e) FE-SEM image of macroporous LDH film with an inverse opal structure prepared via hard templating from LDH NC.

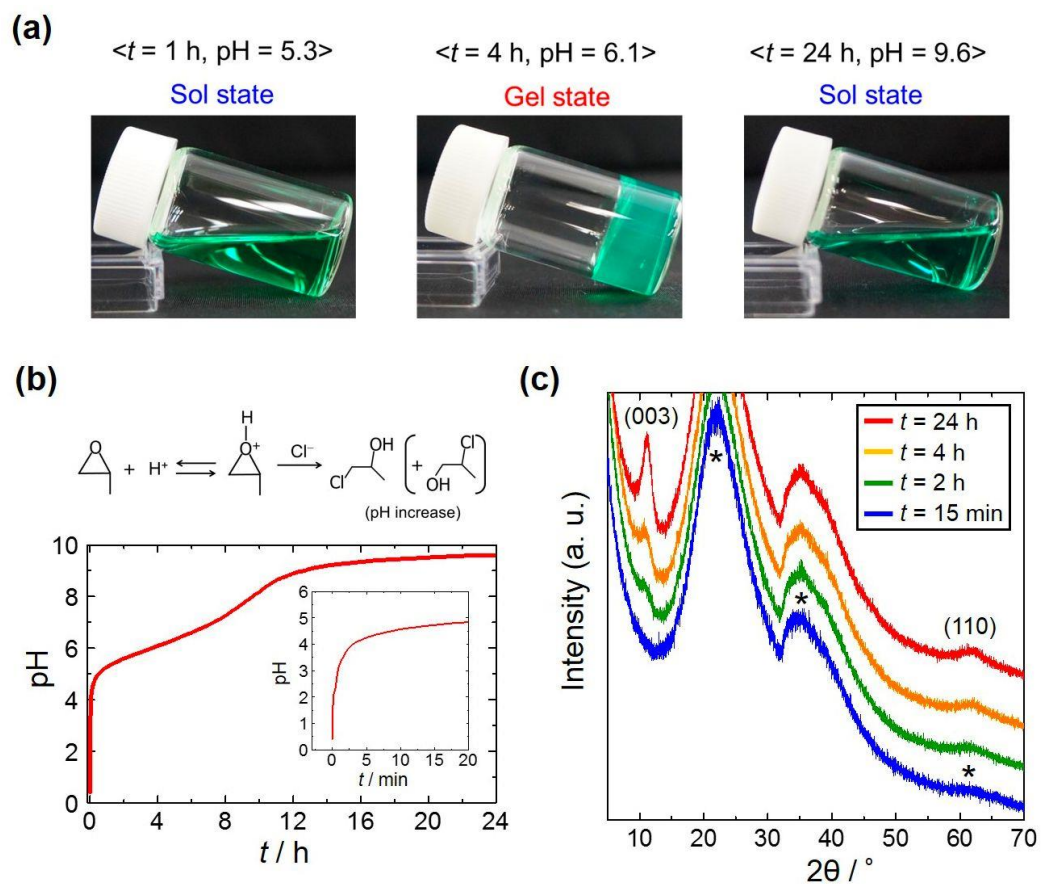


Figure 2. (a) Appearance of the reacting mixture as a function of time. (b) pH evolution of the reaction solution since PO addition ($t = 0$) (c) XRD patterns of the reacting mixture. *: background diffraction from the capillary.

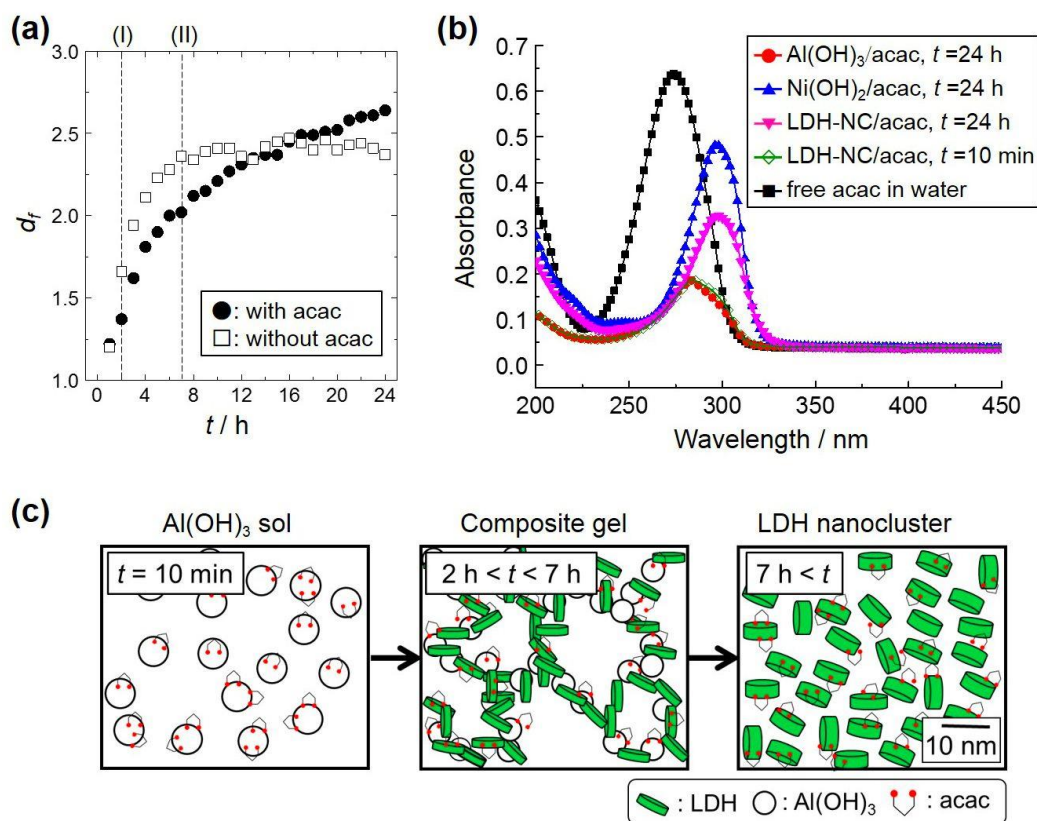
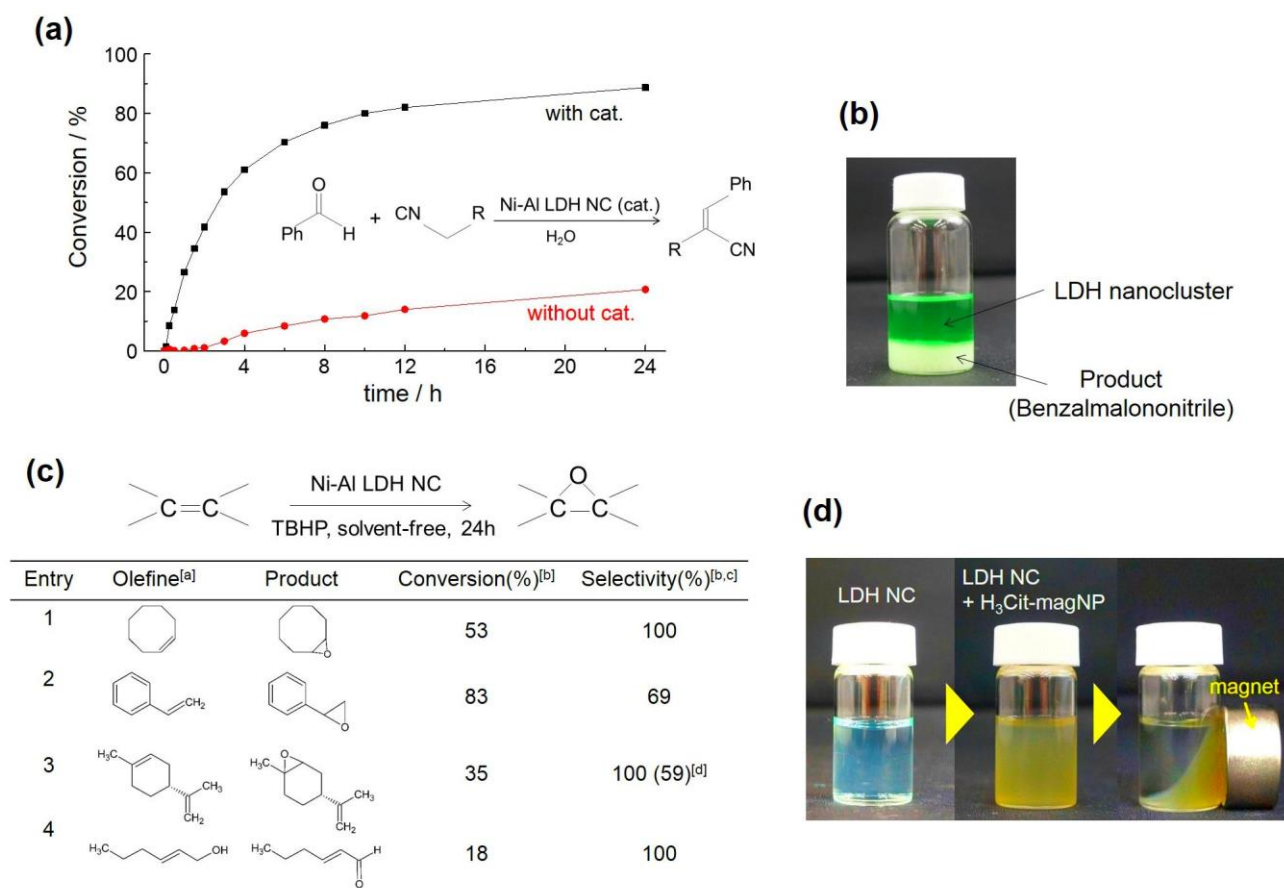


Figure 3. (a) Mass fractal dimension, d_f of the reaction solutions as a function of t for the cases with and without acac. (I) and (II) corresponds the reaction times at which LDH crystallization and deflocculation occurred, respectively. (b) UV-Vis spectra of acac in solutions coexisting with different hydroxides; LDH-NC: LDH nanocluster (Ni/Al=2); Al(OH)₃/acac: hydroxide nanocluster prepared without NiCl₂·6H₂O; Ni(OH)₂/acac: hydroxide nanocluster prepared without AlCl₃·6H₂O; acac: acac in water. (c) Schematic illustration showing the formation mechanism of LDH nanocluster.



^[a]All reactions carried out in the presence of 2 eq. of oxidant (*t*-BuOOH) and 1 mol% of Ni-AI LDH NC at 393 K. Equivalent volume of dibutylether was used as an internal standard. ^[b] Calculated after 24 h. ^[c] Selectivity of Product. ^[d] Selectivity of (Z)-isomer

Figure 4. (a) Kinetic plots for Knoevenagel condensation with and without LDH NC as a catalyst. LDH NC was used as the catalyst after dialysis with deionized water. R=COOC₂H₅ (ethylcyanoacetate). (b) Appearance of the mixture after Knoevenagel condensation between benzaldehyde (10 mmol) and malononitrile (10 mmol). As prepared LDH NC (3 mL) was mixed with EtOH (10 mL) and used as a solvent as well as the catalyst. (c) Summary of epoxidation reaction of olefins catalyzed by LDH NC without solvent. Benzaldehyde (31%) was obtained as a byproduct in the case of entry 2 (d) The collection process of LDH NC by a magnet; LDH NC: LDH nanocluster; H₃Cit-magNP: γ -Fe₂O₃ modified nanoparticles with citric acid. LDH NC was used after dilution for this process.

Table 1 (a) Crystallite size, the presence of impurity phase, and appearance of mixture at $t = 24$ h as a function of acac/Al ratio. (b) Concentration of solutes vs crystallite size. (c) Stability of LDH NC at various degrees of dilution with EtOH.

(a) ¹ acac/Al	acac /mmol	² Purity (single phase)	³ Crystallite size (003) ($t = 24$ h) /nm	at $t = 24$ h	(c) x- fold dilution with EtOH	⁵ Stability of sol
0	0	○	3.1	Gel	x = 1	14 days
0.5	0.625	○	5.4	Gel	2	2 months
0.75	0.938	○	7.6	Sol	4	>3 months
1	1.25	○	5.4	Sol	10	>3 months
1.5	1.88	×	6.1	Sol		
2	2.50	×	7.0	Sol + Precipitates		
4	5.00	×	–	Sol + Precipitates		

(b) ⁴ Relative concentration of solutes	NiCl ₂ ·6H ₂ O /mmol	AlCl ₃ ·6H ₂ O /mmol	acac /mmol	² Purity (single phase)	³ Crystallite size (003) ($t = 3$ months) /nm
1	2.50	1.25	1.25	○	7.1
1/2	1.250	0.625	0.625	○	6.1
1/4	0.625	0.313	0.313	○	4.5
1/10	0.250	0.125	0.125	○	3.6

¹ acac amount was varied as a parameter.

^{2,3} by XRD analysis on powders collected by drying the LDH nanocluster.

⁴ the solvent mixture was set at: H₂O: 1.00 mL; EtOH: 1.50 mL; PO: 1.311 mL.

⁵ time until the suspension lost fluidity.

References

- (1) Polshettiwar, V.; Varma, R. S. *Green Chemistry* **2010**, *12*, 743.
- (2) Rives, V. *Nova Science Publishers, Inc: New York* **2001**.
- (3) Sherman, I. T. *Nova Science Publishers, Inc: New York* **2015**.
- (4) Ebitani, K.; Motokura, K.; Mori, K.; Mizugaki, T.; Kaneda, K. *J. Org. Chem.* **2006**, *71*, 5440.
- (5) Teramura, K.; Iguchi, S.; Mizuno, Y.; Shishido, T.; Tanaka, T. *Angew Chem Int Edit* **2012**, *51*, 8008.
- (6) Mullin, J. W. *Butterworth-Heinemann, Oxford* **2001**.
- (7) Layrac, G.; Destarac, M.; Gerardin, C.; Tichit, D. *Langmuir* **2014**, *30*, 9663.
- (8) Jaramillo, T. F.; Jorgensen, K. P.; Bonde, J.; Nielsen, J. H.; Horch, S.; Chorkendorff, I. *Science* **2007**, *317*, 100.
- (9) Narayanan, R.; El-Sayed, M. A. *J. Phys. Chem. B* **2005**, *109*, 12663.

- (10) Fihri, A.; Bouhrara, M.; Nekoueishahraki, B.; Basset, J. M.; Polshettiwar, V. *Chem. Soc. Rev.* **2011**, *40*, 5181.
- (11) Wang, Q.; O'Hare, D. *Chem. Rev.* **2012**, *112*, 4124.
- (12) Ma, R. Z.; Sasaki, T. *Adv. Mater.* **2010**, *22*, 5082.
- (13) Liu, Z. P.; Ma, R. Z.; Osada, M.; Iyi, N.; Ebina, Y.; Takada, K.; Sasaki, T. *J. Am. Chem. Soc.* **2006**, *128*, 4872.
- (14) Wang, Q.; O'Hare, D. *Chem. Commun.* **2013**, *49*, 6301.
- (15) Chen, C. P.; Wangriya, A.; Buffet, J. C.; O'Hare, D. *Dalton T* **2015**, *44*, 16392.
- (16) Leroux, F.; Adachi-Pagano, M.; Intissar, M.; Chauviere, S.; Forano, C.; Besse, J. P. *J. Mater. Chem.* **2001**, *11*, 105.
- (17) Hibino, T.; Kobayashi, M. *J. Mater. Chem.* **2005**, *15*, 653.
- (18) Wu, Q. L.; Olafsen, A.; Vistad, O. B.; Roots, J.; Norby, P. *J. Mater. Chem.* **2005**, *15*, 4695.
- (19) Malfatti, L.; Tokudome, Y.; Okada, K.; Yagi, S.; Takahashi, M.; Innocenzi, P. *Microporous Mesoporous Mater.* **2012**, *163*, 356.
- (20) Yu, S.; Chow, G. M. *J. Mater. Chem.* **2004**, *14*, 2781.
- (21) Ilavsky, J.; Jemian, P. R. *J. Appl. Crystallogr.* **2009**, *42*, 347.
- (22) Beaucage, G.; Schaefer, D. W. *J. Non-Cryst. Solids* **1994**, *172*, 797.
- (23) Beaucage, G. *J. Appl. Crystallogr.* **1995**, *28*, 717.
- (24) Fernandes, C. I.; Saraiva, M. S.; Nunes, T. G.; Vaz, P. D.; Nunes, C. D. *J. Catal.* **2014**, *309*, 21.
- (25) Oestreicher, V.; Jobbagy, M. *Langmuir* **2013**, *29*, 12104.
- (26) Kuroda, Y.; Miyamoto, Y.; Hibino, M.; Yamaguchi, K.; Mizuno, N. *Chem. Mater.* **2013**, *25*, 2291.
- (27) Wang, C. L. J.; Wu, Y. M. A.; Jacobs, R. M. J.; Warner, J. H.; Williams, G. R.; O'Hare, D. *Chem. Mater.* **2011**, *23*, 171.
- (28) Wang, C. J.; O'Hare, D. *J. Mater. Chem.* **2012**, *22*, 21125.
- (29) *The surface areas of 260-460 m²/g reported for exfoliated LDH powders by the AMOST method was used for the calculation.*
- (30) *BET surface area of 322 m²/g (Figure S3) was used for this calculation*
- (31) Yarger, M. S.; Steinmiller, E. M. P.; Choi, K. S. *Inorg. Chem.* **2008**, *47*, 5859.
- (32) Mondal, D.; Villemure, G. *J. Electroanal. Chem.* **2012**, *687*, 58.
- (33) Faour, A.; Mousty, C.; Prevot, V.; Devouard, B.; De Roy, A.; Bordet, P.; Elkaim, E.; Taviot-Gueho, C. *J Phys Chem C* **2012**, *116*, 15646.
- (34) Geraud, E.; Rafqah, S.; Sarakha, M.; Forano, C.; Prevot, V.; Leroux, F. *Chem. Mater.* **2008**, *20*, 1116.
- (35) Gash, A. E.; Tillotson, T. M.; Satcher, J. H.; Poco, J. F.; Hrubesh, L. W.; Simpson, R. L. *Chem. Mater.* **2001**, *13*, 999.
- (36) Tokudome, Y.; Fujita, K.; Nakanishi, K.; Kanamori, K.; Miura, K.; Hirao, K.; Hanada, T. *J. Ceram. Soc. Jpn.* **2007**, *115*, 925.
- (37) Tokudome, Y.; Tarutani, N.; Nakanishi, K.; Takahashi, M. *Journal of Materials Chemistry A* **2013**, *1*, 7702.
- (38) Tohge, N.; Shinmou, K.; Minami, T. *J. Sol-Gel Sci. Technol.* **1994**, *2*, 581.
- (39) Barnum, D. W. *J. Inorg. Nucl. Chem.* **1961**, *22*, 183.
- (40) Koshimura, H.; Okubo, T. *Anal. Chim. Acta* **1970**, *49*, 67.
- (41) Mahmoud, M. E.; Al Saadi, M. S. M. *Anal. Chim. Acta* **2001**, *450*, 239.
- (42) Osterloh, F. E. *Chem. Mater.* **2008**, *20*, 35.
- (43) Wang, X. C.; Maeda, K.; Thomas, A.; Takanabe, K.; Xin, G.; Carlsson, J. M.; Domen, K.; Antonietti, M. *Nat Mater* **2009**, *8*, 76.

- (44) Pahalagedara, M. N.; Pahalagedara, L. R.; Kuo, C. H.; Dharmarathna, S.; Suib, S. L. *Langmuir* **2014**, *30*, 8228.
- (45) Costantino, U.; Curini, M.; Montanari, F.; Nocchetti, M.; Rosati, O. *J Mol Catal a-Chem* **2003**, *195*, 245.
- (46) Rousselot, I.; Taviot-Gueho, C.; Besse, J. P. *Int. J. Inorg. Mater.* **1999**, *1*, 165.
- (47) Climent, M. J.; Corma, A.; Iborra, S.; Epping, K.; Velty, A. *J. Catal.* **2004**, *225*, 316.
- (48) Murase, T.; Nishijima, Y.; Fujita, M. *J. Am. Chem. Soc.* **2012**, *134*, 162.
- (49) Corma, A.; Martinaranda, R. M. *J. Catal.* **1991**, *130*, 130.
- (50) Shokouhimehr, M.; Piao, Y. Z.; Kim, J.; Jang, Y. J.; Hyeon, T. *Angew Chem Int Edit* **2007**, *46*, 7039.
- (51) Bento, A.; Sanches, A.; Medina, E.; Nunes, C. D.; Vaz, P. D. *Applied Catalysis A: General* **2015**, *504*, 399.
- (52) Bawaked, S.; Dummer, N. F.; Bethell, D.; Knight, D. W.; Hutchings, G. J. *Green Chemistry* **2011**, *13*, 127.
- (53) Sankaranarayanan, S.; Sharma, A.; Srinivasan, K. *Catal Sci Technol* **2015**, *5*, 1187.
- (54) Fernandes, C. I.; Nunes, C. D.; Vaz, P. D. *Current Organic Synthesis* **2012**, *9*, 670.
- (55) Liu, H.; Bai, J.; Li, C. P.; Xu, W.; Sun, W. Y.; Xu, T.; Huang, Y. R.; Li, H. Q. *Rsc Adv* **2014**, *4*, 3195.
- (56) Huang, J. L.; Liu, C.; Sun, D. H.; Hong, Y. L.; Du, M. M.; Odoom-Wubah, T.; Fang, W. P.; Li, Q. B. *Chem. Eng. J.* **2014**, *235*, 215.
- (57) Komarala, E. P.; Nigam, S.; Aslam, M.; Bahadur, D. *New J. Chem.* **2016**, *40*, 423.
- (58) Nigam, S.; Barick, K. C.; Bahadur, D. *J. Magn. Magn. Mater.* **2011**, *323*, 237.